Research article

Song Zhu, Lei Shi*, Shixing Yuan, Ruilong Ma, Xinliang Zhang and Xudong Fan

All-optical controllable electromagnetically induced transparency in coupled silica microbottle cavities

https://doi.org/10.1515/nanoph-2018-0111
Received August 3, 2018; revised August 30, 2018; accepted September 4, 2018

Abstract: An all-optical control scheme of electromagnetically induced transparency (EIT) based on two coupled silica microbottle cavities coated with iron oxide nanoparticles is proposed and experimentally demonstrated. The specially designed and fabricated silica microbottle cavity with a short and spherical end, which is coated with iron oxide nanoparticles, possesses a quality (Q) factor of 1.39×10^8 and large all-optical tunability in a range of 282.32 GHz (2.25 nm) arising from the strong photothermal effect of the nanoparticles. Based on two coupled silica microbottle cavities, we achieve the EIT spectrum with a transparency window bandwidth of 2.3 MHz. The transparency window can be flexibly controlled by tuning the resonant frequency of the higher-Q microcavity. Besides, by tuning the resonant frequencies of the two microcavities separately, the whole EIT spectrum can be shifted with a range of 71.52 GHz, to the best of our knowledge, for the first time. Based on this scheme, we have realized all-optical and independent control of the transparency window and the whole EIT spectrum. We believe this work has great potential in applications such as light storage, optical sensing, and quantum optics.

Keywords: all-optical control; electromagnetically induced transparency; whispering-gallery-mode microcavities; iron oxide nanoparticles.

***Corresponding author: Lei Shi,** Wuhan National Laboratory for Optoelectronics, Huazhong University of Science and Technology, Wuhan 430074, China, e-mail: lshi@hust.edu.cn.
http://orcid.org/0000-0002-9961-6723
Song Zhu, Shixing Yuan, Ruilong Ma and Xinliang Zhang: Wuhan National Laboratory for Optoelectronics, Huazhong University of Science and Technology, Wuhan 430074, China
Xudong Fan: Department of Biomedical Engineering, University of Michigan, 1101 Beal Ave, Ann Arbor, MI 48109, USA

1 Introduction

Electromagnetically induced transparency (EIT) in photonic structures is a phenomenon which arises from the destructive quantum interference effect [1–4] and has potential applications including all-optical switching [5], slow light [6], light storage [7], optical sensing [8], and quantum information processing [9]. In photonic structures, the EIT effect can be realized through several different paths, such as photonic crystals [10], plasmonic nanostructures [11–14], and whispering-gallery-mode (WGM) optical microcavities [15]. WGM optical microcavities are excellent candidates for achieving a narrowband transparency window of the EIT spectrum, due to their high-quality (Q) factors [16–32]. WGM-microcavity-based EIT has been realized in a single microcavity and coupled microcavities. EIT based on a single microcavity has been studied in different kinds of structures, such as microspheres [33], microbottles [34], microbubbles [35], and microtoroids [36, 37]. However, to achieve the EIT effect in a single microcavity, two conditions are required: first, resonance frequencies of two optical modes with different Q factors are close enough to each other; second, there exists energy coupling between them. Furthermore, it is difficult to control the frequency detuning in a large range [34, 35, 37]. Therefore, coupled-microcavity-based EIT has been intensively investigated in recent years. So far, the EIT effect has been illustrated with coupled microspheres [6], coupled microtoroids [15, 38], coupled microtoroid–microdisk [39], and coupled microrings [40]. However, there exist some challenges for these schemes. For coupled microtoroids, it is difficult for the edge-located microtoroid to achieve a Q factor of up to 10^8, which is limited by the fabrication process. Due to low Q factors, silicon-based microcavities cannot be applied when ultrahigh Q factors are required [41]. For coupled microspheres, there is no effective scheme to tune the resonant frequency of a single microsphere.

The silica microbottle cavity, which is fabricated from the standard single-mode fiber (SMF), possesses an

ultrahigh Q factor of ~10^8 and is a good candidate for realizing the EIT effect [42, 43]. Apart from that, the resonance tuning of the microbottle cavity is generally realized by the stretching method [42], which could make the resonant frequencies of two involved WGMs matched. However, the stretching method requires extra piezoelectric bending actuators, and the coupled-microcavity system is easy to be disturbed. In order to avoid this problem, nonmechanical methods ought to be adopted, especially all-optical methods. So far, for the silica microcavity, several all-optical tuning methods have been reported [44–46]. However, those methods lead to degradation of Q factors at different levels and/or realize relatively small tuning ranges. Therefore, it is extremely important to propose an all-optical scheme, which can maintain ultrahigh Q factors during the tuning process and realize a large tuning range.

Here, two coupled silica microbottle cavities coated with iron oxide nanoparticles are proposed and fabricated to achieve all-optical tunable EIT. As shown in Figure 1, the system consists of two coupled silica microbottle cavities, both of which possess short and spherical ends. The original microbottle cavity is fabricated from two SMFs using a fusion splicer [47]. The microbottle cavity with a short and spherical end is fabricated with the help of a carbon dioxide (CO_2) laser. (For details of the CO_2 laser fabrication platform, see part S1 in the Supporting Information). Iron oxide nanoparticles are coated in the tapered area of the microbottle where there is no WGM field distribution. Pump light is fed through the axial direction of the microbottle and absorbed by iron oxide nanoparticles. Due to the strong photothermal effect of iron oxide nanoparticles [48], heat generated in this area is transferred to the locations of WGM fields to change the resonances of the microbottle cavity. In this work, the microbottle cavity with a Q factor of 1.39×10^8 is utilized and the resonant frequency is tuned by 282.32 GHz (2.25 nm @ 1550 nm band), while the ultrahigh Q factor is maintained during the tuning process. By changing the frequency detuning between the two coupled WGMs, we can precisely control the EIT spectrum with a transparency window bandwidth as narrow as 2.3 MHz and a transparency depth of 99%. Especially, we have also realized all-optical control of the whole EIT spectrum in a range of 71.52 GHz by tuning the two microcavities separately.

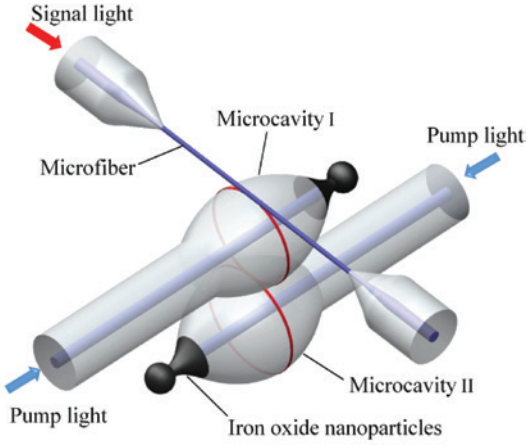

Figure 1: Schematic of all-optical controllable EIT based on coupled silica microbottle cavities.

2 Materials and methods

2.1 Fabrication method

A microbottle fabricated by a fusion splicer is vertically fixed on a three-dimensional (3-D) displacement stage and is attached with a small weight on the bottom. Counterpropagating CO_2 beams are focused on the bottleneck, and a taper emerges due to gravity. Then, we change the locations of the laser beams and obtain a fiber tip. The laser beams are focused on the fiber tip and consequently a spherical end forms. After that, a drop of water-based iron oxide nanoparticle solution is dropped on the surface of a metal platform. By precisely adjusting the relative position between the microbottle and the nanoparticle solution, the spherical end is gradually immerged into and pulled out of the solution. Since there exists a depression between the microcavity and the spherical end, a lot of iron oxide nanoparticles are located in this area after the carrier liquid is evaporated, which can absorb enough pump power.

2.2 Experimental test setup

A tunable laser source (TLS) in the 1550 nm band with a fine scanning range of 30 GHz is utilized in the experiment. Signal light derived from the TLS is controlled by a polarization controller (PC). The signal light is coupled into the microbottle cavity and the transmission light coming from the other end of the microfiber is detected by a photodetector (PD). A digital storage oscilloscope (DSO) is utilized to analyze the transmission spectrum. In order to tune the transparency window, continuous-wave pump light at 1550 nm from a TLS is amplified by a high power erbium-doped fiber amplifier (EDFA) and then is fed into a 10/90 optical splitter through a variable optical attenuator (VOA), which is used to tune the pump power. In order to

control the whole EIT spectrum, two TLSs are needed to pump light into the two microcavities separately.

3 Results and discussion

The equatorial diameters of the higher-*Q* and the lower-*Q* microbottle cavities are 173 μm and 144 μm, respectively. The microfiber with a diameter of around 2.5 μm is utilized as the coupling fiber [49, 50]. Figure 2A shows the fabrication process of the proposed microbottle cavity. Figure 2B shows the fabricated microbottle with a short and spherical end. The coating area seems black because of iron oxide nanoparticles. We also find that there exists a boundary (red line) on the surface of the microbottle, which means the coating range of iron oxide nanoparticles. It could suppress the higher-order WGMs and has no influence on the *Q* factors of the lower-order WGMs. (For details of WGM field distributions, see part S2 in the Supporting Information). Due to the special structure of the microbottle, the guided mode propagating in the fiber core will convert into leaky modes in the tapered area and then absorbed by iron oxide nanoparticles. In order to verify this point, a red beam is fed through the axial direction of the microbottle. As shown in Figure 2C, there exists large light field intensity in the tapered area, which indicates that a lot of optical energy leaks out due to disappearance of the guided mode.

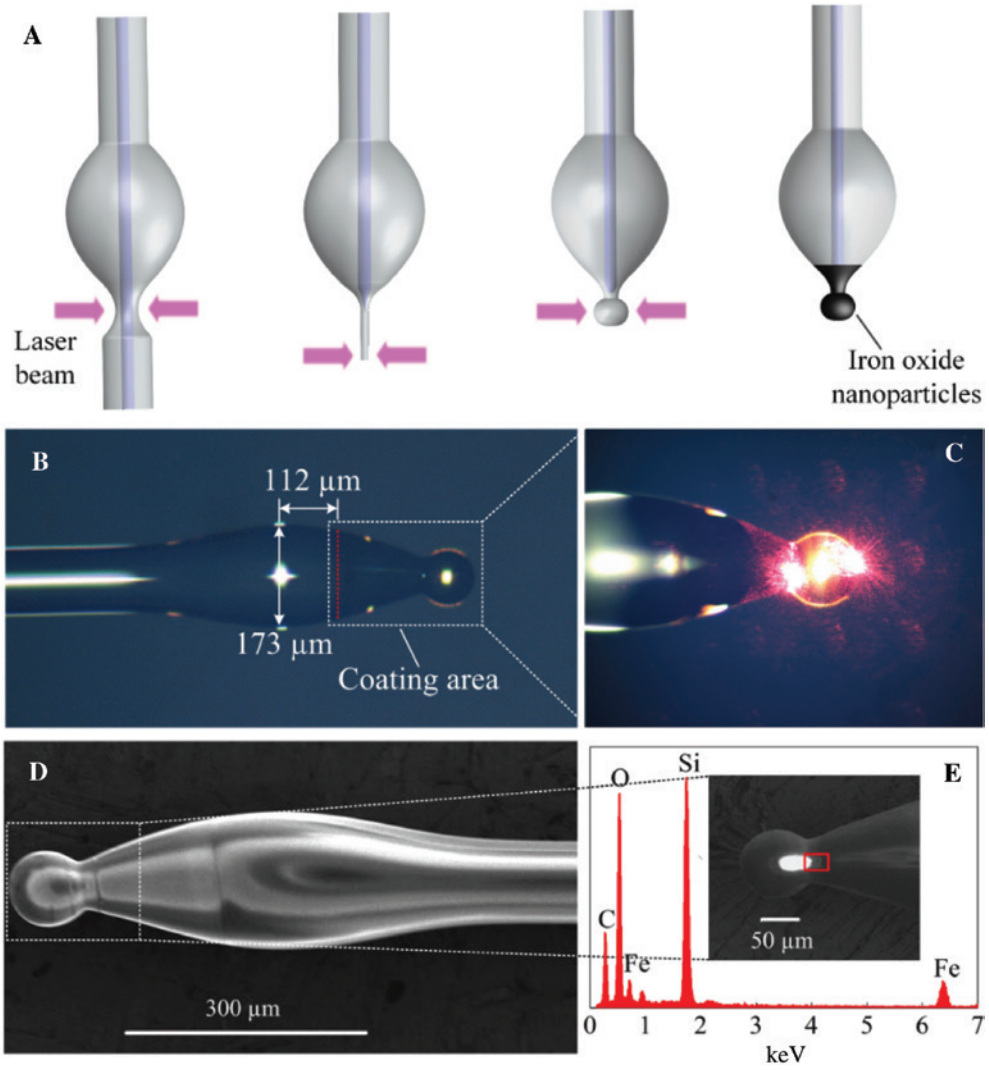

Figure 2: Fabrication process and characterization of the proposed silica microbottle cavity.
(A) Fabrication process of the proposed silica microbottle cavity. (B) Optical micrograph of the higher-*Q* microbottle cavity with a short and spherical end. (C) Close-up view of the coating area. (D) SEM micrograph of the higher-*Q* microbottle cavity. (E) Measured energy dispersive X-ray (EDX) spectroscopy of the tapered area coated with iron oxide nanoparticles. Inset: close-up SEM micrograph of the coating area.

Figure 2D shows the scanning electron micrograph (SEM) of the microbottle. In order to intuitively demonstrate a fact that iron oxide nanoparticles are coated in the tapered area, we measure the energy dispersive X-ray spectroscopy (EDX) of this area, as shown in Figure 2E. The measured area is shown in the red box of the inset, in which more iron oxide nanoparticles exist. There are several obvious peaks in the spectroscopy result, which represent the

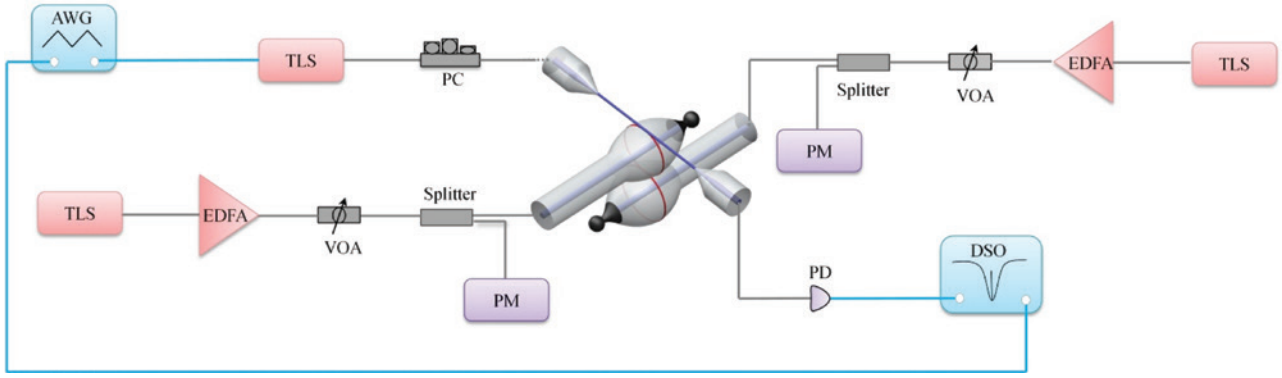

Figure 3: Experimental setup for performance test of all-optical controllable EIT.
AWG: arbitrary waveform generator. TLS: tunable laser source, PC: polarization controller, PD: photodetector, DSO: digital storage oscilloscope, EDFA: erbium-doped fiber amplifier, VOA: variable optical attenuator, PM: power meter.

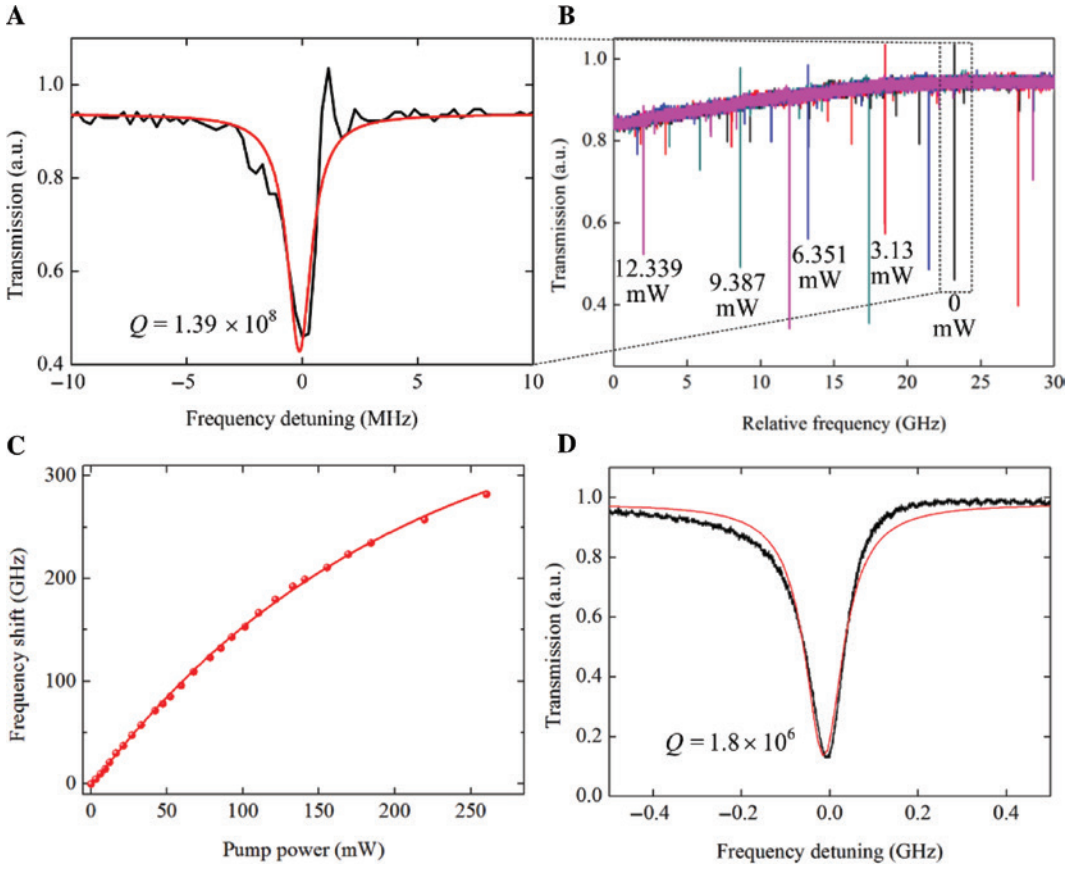

Figure 4: Optical performance and tunability of the fabricated microbottle cavity.
(A) Transmission spectrum of a single resonance mode of the higher-*Q* microbottle cavity. The red line is corresponding Lorentzian fitting. (B) 30-GHz range transmission spectra of the higher-*Q* microbottle cavity with different pump powers. (C) Resonant frequency shift versus the pump power, with the measured data in the red dot and the fitted data in the red line. (D) Transmission spectrum of a single resonance mode of the lower-*Q* microbottle cavity. The red line is corresponding Lorentzian fitting.

consistence of the atomic ratio of oxygen (O), ferrum (Fe), silicon (Si), and carbon (C), and this indicates that there are only iron oxide nanoparticles on the microcavity. The existence of carbon is due to the conductive plastic around the end, which can enhance its conductivity.

The EIT spectrum of the coupled microcavities can be explained by coupled mode equations:

$$\frac{da^{CW}}{dt}=\left(i\Delta\omega_a-\frac{1}{2\tau}\right)a^{CW}-i\mu b^{CCW}+\sqrt{\kappa_{ex}S_{in}} \quad (1)$$

$$\frac{db^{CCW}}{dt}=\left(i\Delta\omega_b-\frac{1}{2\tau_o}\right)b^{CCW}-i\mu a^{CW} \quad (2)$$

$$S_{\text{out}}=S_{\text{in}}-\sqrt{\kappa_{ex}}a^{CW} \quad (3)$$

$$T=\left|\frac{S_{\text{out}}}{S_{\text{in}}}\right|^2 \quad (4)$$

where a^{CW} and b^{CCW} are the mode field amplitudes in the two microcavities, τ and τ_o represent the total and intrinsic lifetimes of photons in the two microcavities, κ_{ex} denotes the coupling strength between the microfiber and the lower-Q microcavity, μ is the coupling strength between a^{CW} and b^{CCW} modes, $\Delta\omega_{a/b}=\omega-\omega_{a/b}$ are the frequency detunings in the two microcavities, S_{in} and S_{out} represent the incident and transmitted light field amplitudes, T denotes the transmission coefficient of the signal light. By combining Eqs. (1), (2), (3), and (4), T can be expressed as:

$$T=\left[1-\frac{2\tau\kappa_{ex}-i4\tau\tau_o\kappa_{ex}\Delta\omega_b}{-4\tau\tau_o\Delta\omega_a\Delta\omega_b-i2\tau_o\Delta\omega_b-i2\tau\Delta\omega_a+1+4\tau\tau_o\mu^2}\right]^2 \quad (5)$$

From Eq. (5), we can find that the transmission coefficient T depends on $\Delta\omega_{a/b}$ and μ. We first measure the Q factor and the tuning performance of the higher-Q microbottle cavity based on Figure 3. Figure 4A shows the measured transmission spectrum of a single resonance mode, which possesses a loaded Q factor of 1.39×10^8 by Lorentzian fitting. The apparent ring down phenomenon results from the ultrahigh Q factor of the microcavity [51]. For achieving controllable EIT, the tunability of a single microcavity is critical. Therefore, we also test the all-optical tuning performance of the microcavity, as shown in Figure 4B and C. Heat generated in the tapered area is transmitted to the microcavity. Due to the positive thermo-optic and thermal expansion coefficients of silica, the resonant frequency generates the redshift [44–46]. (For details of the response time of the tuning process, see part S3 in the Supporting Information). Figure 4B shows the transmission spectra at different pump powers in a small range, and there still exist apparent ring down phenomena in the transmission spectra. Meanwhile, we find that the ultrahigh Q factor of the microcavity is still maintained during the tuning process. As shown in Figure 4C, the red circle dotted line represents the resonant frequency shift with the pump power. A total tuning range of 282.32 GHz (2.25 nm) is achieved as the pump power increases to 260.28 mW. The overcoupling condition between the microfiber and the lower-Q microcavity is reached by enabling them to get in touch with each other, which also can make the coupling system stable. Figure 4D represents the

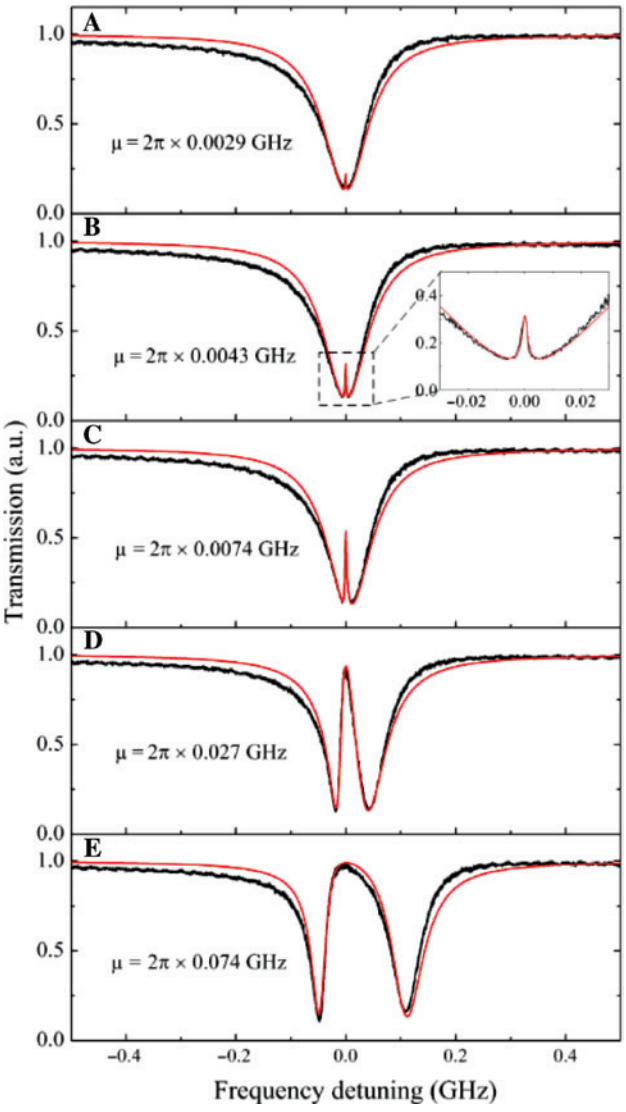

Figure 5: Transmission spectra for different gaps between the coupled microcavities.
(A–E) Measured EIT spectra (black lines) of the coupled microcavities for different coupling strengths. (Inset) Close-up to the transparency window with a bandwidth of 2.3 MHz. Theoretical fittings are represented by the red lines calculated from Eq. (5) and in excellent agreement with the experimental results.

transmission spectrum of the lower-Q microcavity with a loaded Q factor of 1.8×10^6. The red line represents Lorentzian fitting. The measured asymmetric spectrum may result from the excitation of spiral modes in the microcavity [52].

To obtain the EIT spectrum, the two microcavities are fixed on two three-dimensional displacement stages and couple with each other. In order to optimize the depth and the bandwidth of the transparency window, we can control the EIT spectrum by changing the coupling gap between the two microcavities. When the microfiber couples with the lower-Q microcavity, which is away from the higher-Q microcavity, there is only the transmission spectrum of the lower-Q microcavity. Then, we gradually decrease the gap between the two microcavities. In Figure 5A, when the gap is adjusted to a specific value, a narrow transparent window appears in the center of the lower-Q mode due to destructive interference between two optical pathways in the coupled microcavities [6]. Then, the gap is keeping decreased. From Figure 5A–E, it can be seen that both the transparency peak and the bandwidth gradually increase as the calculated coupling strength increases from $2\pi\times0.0029$ to $2\pi\times0.074$ GHz. The red lines represent the theoretical fitting calculated from Eq. (5), which is well agreed with the experimental results. Besides, due to the ultrahigh Q factor of the higher-Q microcavity, the bandwidth of the transparency window achieves 2.3 MHz,

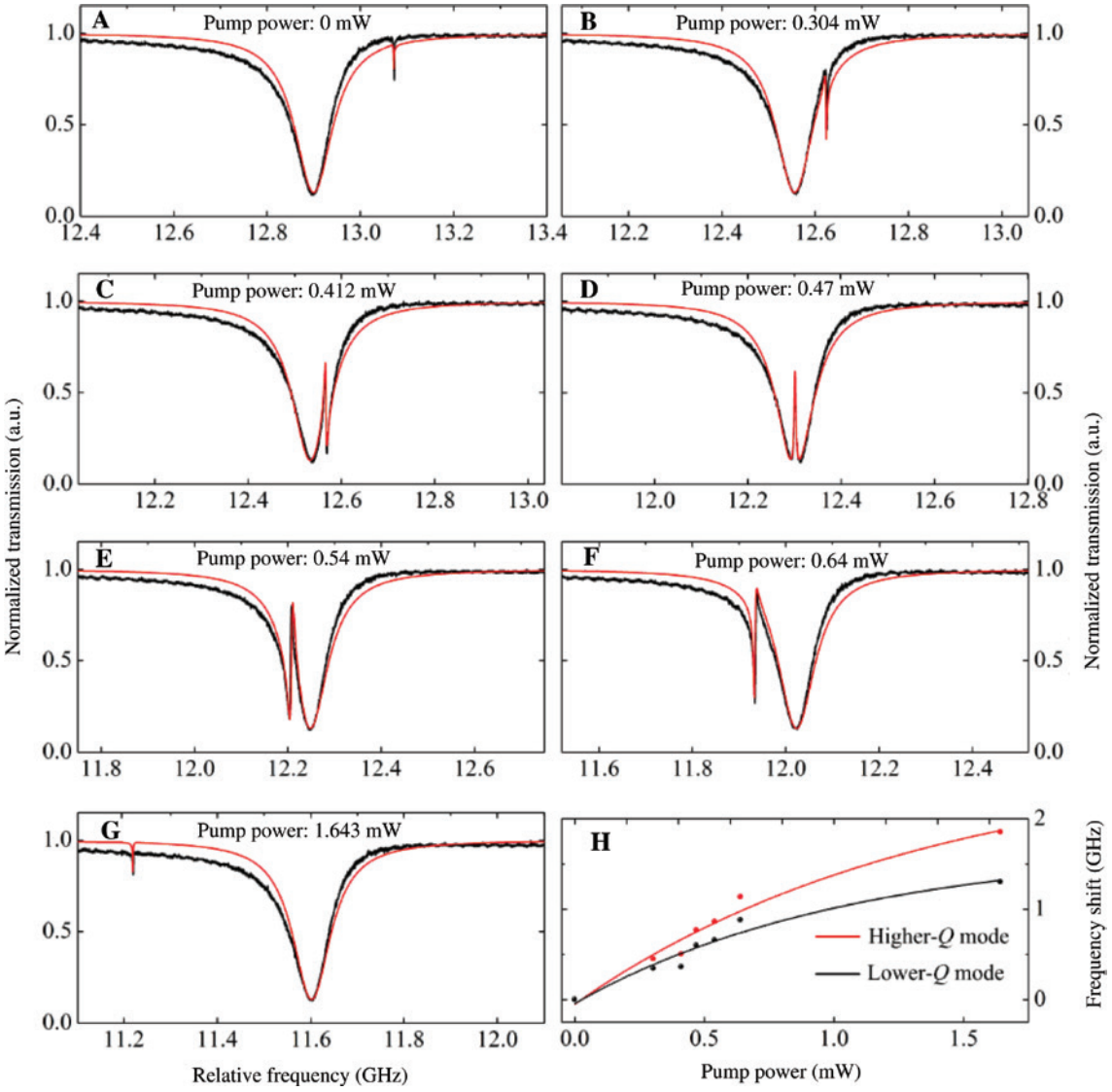

Figure 6: Transmission spectra for different frequency detunings between the coupled WGMs.
(A–G) Measured EIT spectra (black lines) of the coupled microcavities for different pump powers. Frequency detunings are 171.07, 65.89, 30.36, 0, −33, −83.61, and −381.02 MHz, respectively. (H) Frequency shifs of the higher-Q and the lower-Q modes as a function of the pump power.

which is the narrowest compared with the previous work based on microcavities [6, 33–35, 37–40], as shown in Figure 5B. From Figure 5E, as the gap is further decreased, the transmission spectrum splits into two separate dips and the maximum transparency depth of 99% is achieved. However, the bandwidth of the transparency window is about 115.4 MHz, which may result from the loss induced by the large coupling strength [6]. Besides, the transmission phase shift of the EIT spectrum, which indicates the change of the coupling strength, is also calculated based on the measured transmission spectrum. (For details of the transmission phase shift, see part S4 in the Supporting Information).

After that, we demonstrate the all-optical tuning of the transparency window. The transparency window is derived from the presence of the higher-*Q* microcavity and thus can be precisely controlled by changing its resonant frequency. Figure 6A shows the transmission spectrum with two independent dips, and the frequency detuning of the two modes is 171.07 MHz, when there is no pump power to the higher-*Q* microcavity. Then, pump light is fed into the axial direction of the higher-*Q* microcavity. As shown in Figure 6B and C, as the increase of the pump power, the frequency detuning decreases, and the Lorentzian line shape evolves to the asymmetric Fano resonance line shape. As the pump power increases to 0.47 mW, the frequency detuning is reduced to zero, and the asymmetry of the Fano resonance disappears while the EIT spectrum emerges. As the pump power further increases, the frequency detuning increases and the asymmetric line shape appears again, as shown in Figure 6E and F. Finally, two modes with the Lorentzian line shapes and the frequency detuning of 381.02 MHz appear again as the pump power increases to 1.64 mW. We find that the coupling strength in Figure 6G is larger than that in Figure 6A, because the thermal expansion will lead to the increase of the microcavity diameter, and then the decrease of the gap between the coupled microcavities. Furthermore, we also find that, though only the higher-*Q* microcavity is pumped, the resonant frequency of the lower-*Q* microcavity also changes a little. It is because that heat generated in the higher-*Q* microcavity is transferred to the lower-*Q* microcavity, leading to the redshift of its resonant frequency. In Figure 6H, the tuning sensitivity of the lower-*Q* microcavity is smaller than that of the higher-*Q* microcavity, because a smaller portion of the generated heat is transferred to the lower-*Q* microcavity, when only the higher-*Q* microcavity is pumped.

Since the lower-*Q* microcavity is also coated with iron oxide nanoparticles, its resonant frequency can be tuned

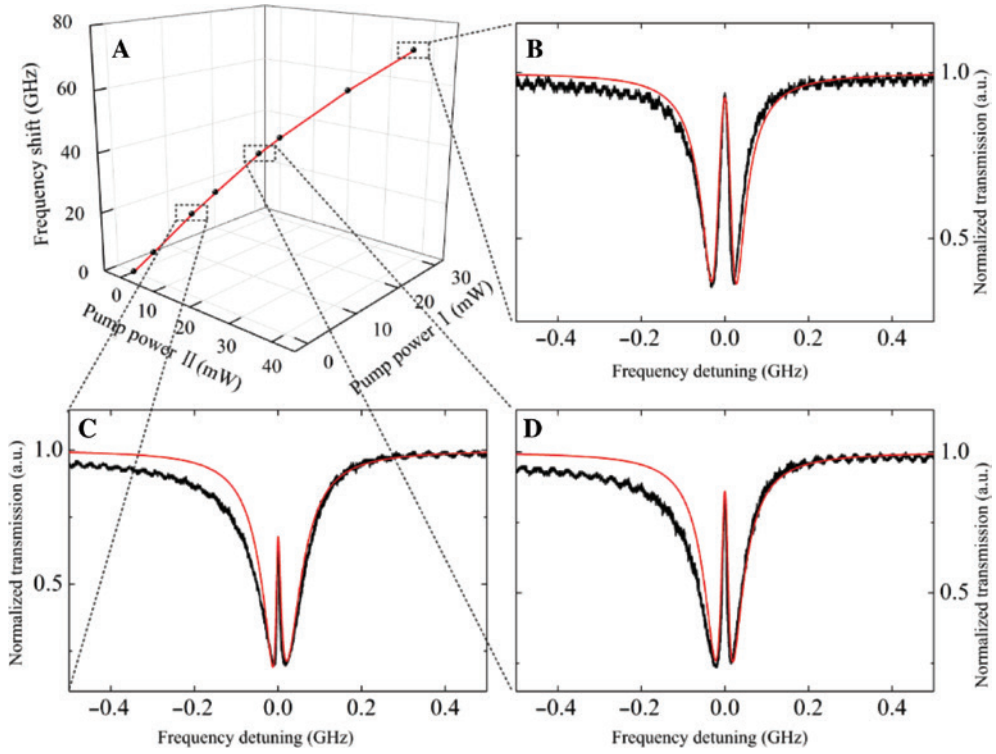

Figure 7: Tuning of the whole EIT spectrum.
(A) Frequency shift of the whole EIT spectrum as a function of the pump power (pump power I in the lower-*Q* microcavity; pump power II in the higher-*Q* microcavity). (B–D) Three specific EIT spectra with different pump powers.

by pumping light through its axial direction. Therefore, the whole EIT spectrum can be controlled by feeding the pump light through the axial directions of the lower-*Q* and the higher-*Q* microcavities. The frequency detuning can be precisely controlled by separately tuning the two microcavities with different pump powers. From Figure 7A, by increasing the pump powers of the two microcavities, the whole EIT spectrum can be shifted by 71.52 GHz. We also find that the tuning sensitivities of the two microcavities are slightly different, because the sizes and the mode orders of the two microcavities are different. It is the first time to all-optically control the whole EIT spectrum compared with reported studies [33–40]. Figure 7B–D are three specific EIT spectra at different pump powers, which demonstrate that the EIT spectrum profile can always be maintained during the tuning process. When the EIT spectrum is located at a specific resonant frequency, the transparency window can be flexibly shifted due to the large tunability of the higher-*Q* microcavity. Based on this method, a specific EIT spectrum can emerge in a relatively large frequency range. In this way, based on two tunable and coupled microcavities, it is possible for us to realize all-optical control of the transparency window and the whole EIT spectrum.

4 Conclusion

In conclusion, we achieved all-optical controllable EIT based on two coupled silica microbottle cavities coated with iron oxide nanoparticles. Due to the large tunability, we achieved all-optical control of the transparency window. Due to the ultrahigh-*Q* factor of the microcavity, a transparency depth of 99% and a transparency window bandwidth as narrow as 2.3 MHz were obtained. Besides, we realized all-optical control of the whole EIT spectrum with a range of 71.52 GHz for the first time. Therefore, based on this scheme, the transparency window and the whole EIT spectrum can be all-optically and independently controlled. We believe this work can be utilized in optical sensing, slow light, and quantum optics.

Funding: National Natural Science Foundation of China (Grant Nos. 11774110 and 61307075); National Key Research and Development Program of China (Grant No. 2016YFB0402503); State Key Laboratory of Advanced Optical Communication Systems and Networks, Shanghai Jiao Tong University, China (Grant No. 2018GZKF03002).

References

[1] Harris SE. Induced transparency. Phys Today 1997;50:36.
[2] Opatrný T, Welsch DG. Coupled cavities for enhancing the cross-phase-modulation in electromagnetically induced transparency. Phys Rev A 2001;64:023805.
[3] Naweed A, Farca G, Shopova SI, Rosenberger AT. Induced transparency and absorption in coupled whispering-gallery microresonators. Phys Rev A 2005;71:043804.
[4] Liu YC, Li BB, Xiao YF. Electromagnetically induced transparency in optical microcavities. Nanophotonics 2017;6:789–811.
[5] Fan SH. Sharp asymmetric line shapes in side-coupled waveguide-cavity systems. Appl Phys Lett 2002;80:908–10.
[6] Totsuka K, Kobayashi N, Tomita M. Slow light in coupled-resonator-induced transparency. Phys Rev Lett 2007;98:213904.
[7] Xu QF, Dong P, Lipson M. Breaking the delay-bandwidth limit in a photonic structure. Nat Phys 2007;3:406–10.
[8] Peng C, Li ZB, Xu AS. Optical gyroscope based on a coupled resonator with the all-optical analogous property of electromagnetically induced transparency. Opt Express 2007;15:3864–75.
[9] Di K, Xie CD, Zhang J. Coupled-resonator-induced transparency with a squeezed vacuum. Phys Rev Lett 2011;106:153602.
[10] Yang XD, Yu MB, Kwong DL, Wong CW. All-optical analog to electromagnetically induced transparency in multiple coupled photonic crystal cavities. Phys Rev Lett 2009;102:173902.
[11] Liu N, Langguth L, Weiss T, et al. Plasmonic analogue of electromagnetically induced transparency at the Drude damping limit. Nat Mater 2009;8:758–62.
[12] Liu N, Weiss T, Mesch M, et al. Planar metamaterial analogue of electromagnetically induced transparency for plasmonic sensing. Nano Lett 2010;10:1103–7.
[13] Zhang S, Genov D, Wang Y, Liu M, Zhang X. Plasmon-induced transparency in metamaterials. Phys Rev Lett 2008;101:047401.
[14] Luk'yanchuk B, Zheludev NI, Maier SA, et al. The Fano resonance in plasmonic nanostructures and metamaterials. Nat Mater 2010;9:707–15.
[15] Peng B, Ozdemir SW, Chen WJ, Nori F, Yang L. What is and what is not electromagnetically induced transparency in whispering-gallery microcavities. Nat Commun 2014;5:5082.
[16] Kippenberg TJ, Spillane SM, Vahala KJ. Kerr-nonlinearity optical parametric oscillation in an ultrahigh-Q toroid microcavity. Phys Rev Lett 2004;93:083904.
[17] Park Y, Cook AK, Wang HL. Cavity QED with diamond nanocrystals and silica microspheres. Nano Lett 2006;6:2075–9.
[18] Götzinger S, Menezes DSL, Mazzei A, Kühn S, Sandoghdar V, Benson O. Controlled photon transfer between two individual nanoemitters via shared high-Q modes of a microsphere resonator. Nano Lett 2006;6:1151–4.
[19] Vollmer F, Yang L. Label-free detection with high-Q microcavities: a review of biosensing mechanisms for integrated devices. Nanophotonics 2012;1:267–91.
[20] Toren P, Ozgur E, Bayindir M. Oligonucleotide-based label-free detection with optical microresonators: strategies and challenges. Lab Chip 2016;16:2572–95.
[21] Yang SC, Wang Y, Sun HD. Advances and prospects for whispering gallery mode microcavities. Adv Optical Mater 2015;3:1136–62.

[22] Shen Z, Zhang YL, Chen Y, et al. Experimental realization of optomechanically induced non-reciprocity. Nat Photonics 2016;10:657–61.
[23] Xavier J, Vincent S, Meder F, Vollmer F. Advances in optoplasmonic sensors-combining optical nano/microcavities and photonic crystals with plasmonic nanostructures and nanoparticles. Nanophotonics 2018;7:1–38.
[24] Klusmann C, Oppermann J, Forster P, Rockstuhl C, Kalt H. Identification of dielectric, plasmonic, and hybrid modes in metal coated whispering-gallery-mode resonators. ACS Photonics 2018;5:2365–73.
[25] Jiang XF, Shao LB, Zhang SX, et al. Chaos-assisted broadband momentum transformation in optical microresonators. Science 2017;358:344–7.
[26] Zhang N, Gu ZY, Liu S, et al. Far-field single nanoparticle detection and sizing. Optica 2017;4:1151–6.
[27] Heylman KD, Knapper KA, Horak EH, Rea MT, Vanga SK, Goldsmith RH. Optical microresonators for sensing and transduction: a materials perspective. Adv Mater 2017;29:1700037.
[28] Suh MG, Yang QF, Yang KY, Yi X, Vahala KJ. Microresonator soliton dual-comb spectroscopy. Science 2016;354:600–3.
[29] Kim E, Baaske MD, Schuldes I, Wilsch PS, Vollmer F. Label-free optical detection of single enzyme-reactantreactions and associated conformational changes. Sci Adv 2017;3:e1603044.
[30] Shen X, Beltran, RC, Diep VM, Soltani S, Armani AM. Low-threshold parametric oscillation in organically modified microcavities. Sci Adv 2018;4:eaao4507.
[31] Liu S, Sun WZ, Wang YJ, et al. End-fire injection of light into high-Q silicon microdisks. Optica 2018;5:612–6.
[32] Spencer DT, Drake T, Briles TC, et al. An optical-frequency synthesizer using integrated photonics. Nature 2018;557: 81–5.
[33] Zheng YL, Yang JF, Shen ZH, et al. Optically induced transparency in a micro-cavity. Light Sci Appl 2016;5:e16072.
[34] Wang Y, Zhang K, Zhou S, Wu YH, Chi MB, Hao P. Coupled-mode induced transparency in a bottle whispering-gallery-mode resonator. Opt Lett 2016;41:1825–8.
[35] Yang Y, Saurabh S, Ward J, Chormaic SN. Coupled-mode-induced transparency in aerostatically tuned microbubble whispering-gallery resonators. Opt Lett 2015;40:1834–7.
[36] Weis S, Rivière R, Deléglise S, et al. Optomechanically induced transparency. Science 2010;330:1520–3.
[37] Xiao YF, He LN, Zhu JG, Yang L. Electromagnetically induced transparency-like effect in a single polydimethylsiloxane-coated silica microtoroid. Appl Phys Lett 2009;94:231115.
[38] Yoshiki W, Honda Y, Tetsumoto T, Furusawa K, Sekine N, Tanabe T. All-optical tunable buffering with coupled ultra-high Q whispering gallery mode microcavities. Sci Rep 2017;7:10688.
[39] Li GY, Jiang XS, Hua SY, Qin YC, Xiao M. Optomechanically tuned electromagnetically induced transparency-like effect in coupled optical microcavities. Appl Phys Lett 2016;109:261106.
[40] Xu QF, Sandhu S, Povinelli ML, Shakya J, Fan SH, Lipson M. Experimental realization of an on-chip all-optical analogue to electromagnetically induced transparency. Phys Rev Lett 2006;96:123901.
[41] Soltani M, Yegnanarayanan S, Adibi A. Ultra-high Q planar silicon microdisk resonators for chip-scale silicon photonics. Opt Express 2007;15:4694–704.
[42] Pöllinger M, O'Shea D, Warken F, Rauschenbeutel A. Ultrahigh-tunable whispering-gallery-mode microresonator. Phys Rev Lett 2009;103:053901.
[43] Asano M, Takeuchi Y, Chen WJ, et al. Observation of optomechanical coupling in a microbottle resonator. Laser Photon Rev 2016;10:603–11.
[44] Liu Y, Shi L, Xu XB, et al. All-optical tuning of a magnetic-fluid-filled optofluidic ring resonator. Lab Chip 2014;14:3004–10.
[45] Bo F, Wang J, Cui J, et al. Lithium-niobate-silica hybrid whispering-gallery-mode resonators. Adv Mater 2015;27:8075–81.
[46] Zhu S, Shi L, Yuan SX, Xu XB, Zhang XL. All-optical control of ultrahigh-Q silica microcavities with iron oxide nanoparticles. Opt Lett 2017;42:5133–6.
[47] Murugan GS, Wilkinson JS, Zervas MN. Selective excitation of whispering gallery modes in a novel bottle microresonator. Opt Express 2009;17:11916–25.
[48] Schlegel A, Alvarado SF, Wachter P. Optical properties of magnetite (Fe_3O_4). J Phys C Solid State Phys 1979;12:1157.
[49] Zhao P, Shi L, Liu Y, Wang ZQ, Zhang XL. Compact in-line optical notch filter based on an asymmetric microfiber coupler. Appl Opt 2013;52:8834–9.
[50] Wang KY, Gu ZY, Sun WZ, Li JK, Xiao SM, Song QH. Quasi-guiding Modes in Microfibers on a High Refractive Index Substrate. ACS Photonics 2015;2:1278–83.
[51] Trebaol S, Dumeige Y, Féron P. Ringing phenomenon in coupled cavities: application to modal coupling in whispering-gallery-mode resonators. Phys Rev A 2010;81:043828.
[52] Zamora V, Díez A, Andrés MV, Gimeno B. Refractometric sensor based on whispering-gallery modes of thin capillaries. Opt Express 2007;15:12011–6.

Supplementary Material: The online version of this article offers supplementary material (https://doi.org/10.1515/nanoph-2018-0111).